Demonstration of calibration-free WMS measurement of gas parameters with in-situ real-time characterization of laser parameters using cw-DFB-QCL, VCSEL and DFB lasers

Abhishek Upadhyay[1,2], David Wilson[2], Michael Lengden[2], Arup Lal Chakraborty[1,*], George Stewart[2] and Walter Johnstone[2]

[1] *Electrical Engineering, Indian Institute of Technology Gandhinagar, Palaj - 382355, Gandhinagar, Gujarat, India*

[2] *Centre for Microsystems and Photonics, University of Strathclyde, Glasgow, UK*

[*] *arup@iitgn.ac.in*

Abstract: This paper presents a detailed experimental and theoretical study of a new calibration-free n^{th} harmonic wavelength modulation spectroscopy approach and demonstrates that it is applicable to various types of semiconductor lasers that are widely used in near-infrared and mid-infrared tunable diode laser spectroscopy. A 5250 nm continuous wave distributed feedback quantum cascade laser is used to extract the concentration and pressure values of nitric oxide using 2f WMS technique under controlled conditions. The applicability of the technique to different types of current tuned semiconductor lasers is demonstrated by extending it to a 2004 nm vertical cavity surface emitting laser and a 1650 nm distributed feedback edge-emitting laser to extract gas parameters of carbon dioxide and methane respectively. The generality of the technique is demonstrated by extending it to third harmonic detection for the three different kinds of lasers used in this study. The methodology required to provide in-situ real-time measurements of both gas parameters and operating characteristics of the laser is described in detail. Finally, the advantages and limitations of the technique are discussed in view of the fact that the characteristic behaviour of the laser sources is somewhat different. We specifically discuss the issue of targeting non-absorbing wavelength regions and the choice of modulation frequency and modulation amplitude of the laser as well as the choice of the detection harmonic.

OCIS codes: (300.6380) Spectroscopy, modulation; (280.4788) Optical sensing and sensors; (140.3600) Lasers, tunable; (010.1030) Absorption; nf Wavelength Modulation Spectroscopy; cw-DFB-QCL.

References and links

1. O. Witzel, A. Klein, C. Meffert, S. Wagner, S. Kaiser, C. Schulz, and V. Ebert, "VCSEL-based, high-speed, in situ TDLAS for in-cylinder water vapor measurements in IC engines," Opt. Express **21**, 19951-19965 (2013).
2. T. Aizawa, "Diode-laser wavelength-modulation absorption spectroscopy for quantitative in situ measurements of temperature and OH radical concentration in combustion gases," Appl. Opt. **40**, 4894–4903 (2001).

3. K. Sun, R. Sur, X. Chao, J. B. Jeffries, R. K. Hanson, R. J. Pummill, K. J. Whitty, "TDL absorption sensors for gas temperature and concentrations in a high-pressure entrained-flow coal gasifier," Proceedings of the Combustion Institute **34**, 3593–3601 (2013).
4. C. S. Goldenstein, I. A. Schultz, R. M. Spearrin, J. B. Jeffries, R. K. Hanson, "Scanned-wavelength-modulation spectroscopy near 2.5 m for H2O and temperature in a hydrocarbon-fueled scramjet combustor," Appl. Phys. B **116**, 717–727, (2014).
5. Y. Gerard, R. J. Holdsworth, P. A. Martin, "Multispecies in situ monitoring of a static internal combustion engine by near-infrared diode laser sensors," Appl. Opt. **46**, 3937–3945 (2007).
6. M. F. Miller, W. J. Kessler, M. G. Allen, "Diode laser-based air mass flux sensor for subsonic aero-propulsion inlets, Appl. Opt. **35**, 905–4912 (1996).
7. M. Lengden, R. Cunningham and W. Johnstone, "Tunable diode laser gas analyser for methane measurements on a large scale solid oxide fuel cell," Journal of Power Sources **196**, 8406–8408 (2011).
8. D.J. Miller, K. Sun, L. Tao, M.A. Khan, and M.A. Zondlo, "Open-path, quantum cascade-laser-based sensor for high-resolution atmospheric ammonia measurements," Atmos. Meas. Tech. **7**, 81–93 (2014).
9. K. Sun, L. Tao, D. J. Miller, M. A. Khan, and M. A. Zondlo, "On-road ammonia emissions characterized by mobile open-path measurements," Envir. Sci Technol. **48**(7), 3943–3950 (2014).
10. Y. Cao, N. P. Sanchez, W. Jiang, R. J. Griffin, F. Xie, L. C. Hughes, C. Zah, and F. K. Tittel, "Simultaneous atmospheric nitrous oxide, methane and water vapor detection with a single continuous wave quantum cascade laser," Opt. Express **23**, 2121–2132 (2015).
11. G. B. Rieker, J. B. Jeffries, R. K. Hanson, "Calibration-free wavelength-modulation spectroscopy for measurements of gas temperature and concentration in harsh environments," Appl. Opt. **48**, 5546–5559 (2009).
12. A. Farooq, J. B. Jeffries, R. K. Hanson, "Measurements of CO2 concentration and temperature at high pressures using 1f-normalized wavelength-modulation spectroscopy with second harmonic detection near 2.7m," Appl. Opt. **48**, 6740–6753 (2009).
13. X. Chao, J. B. Jeffries, R. K. Hanson, "Wavelength-modulation-spectroscopy for real-time, in situ NO detection in combustion gases with a 5.2m quantum-cascade laser, " Appl. Phys. B **106**, 987–997 (2012).
14. K. Sun, X. Chao, R. Sur, C. S. Goldenstein, J. B. Jeffries and R. K. Hanson, "Analysis of calibration-free wavelength-scanned wavelength modulation spectroscopy for practical gas sensing using tunable diode lasers," Meas. Sci. Technol. **24**, 125203 (2013).
15. C. S. Goldenstein, C. L. Strand, I. A. Schultz, K. Sun, J. B. Jeffries, and R. K. Hanson, "Fitting of calibration-free scanned-wavelength-modulation spectroscopy spectra for determination of gas properties and absorption lineshapes," Appl. Opt. **53**, 356–367 (2014).
16. A. Upadhyay and A. L. Chakraborty, "Calibration-free 2f WMS with in situ real time characterization of a laser modulated at its phase quadrature and with 2f RAM nulling," Opt. Lett. **40**, 4086–4089 (2015).
17. J. R. P. Bain, W. Johnstone, K. Ruxton, G. Stewart, M. Lengden, and K. Duffin, "Recovery of absolute gas absorption line shapes using tunable diode laser spectroscopy with wavelength modulation - part 2: experimental investigation," J. Lightwave Technol. **29**, 987–996 (2011).
18. A. Upadhyay, A. L. Chakraborty, "Residual amplitude modulation method implemented at the phase quadrature frequency of a 1650-nm laser diode for line shape recovery of methane," Sensors Journal, IEEE **15**, 1153–1160 (2015).
19. A. J. McGettrick, K. Duffin, W. Johnstone, G. Stewart, D. G. Moodie, "Tunable diode laser spectroscopy with wavelength modulation: a phasor decomposition method for calibration-fee measurements of gas concentration and pressure," IEEE J. Lightwav. Technol. **26**, 432–440 (2008).
20. A. L. Chakraborty, K. Ruxton, W. Johnstone, "Suppression of intensity modulation contributions to signals in second harmonic wavelength modulation spectroscopy," Opt. Lett. **35**, 2400–2402 (2010).
21. D. Richter, A. Fried, B. P. Wert, J. G. Walega, and F. K. Tittel, "Development of a tunable mid-IR difference frequency laser source for highly sensitive airborne trace gas detection," Appl. Phys. B **75**, 281–288 (2002).
22. J. Chen, A. Hangauer, R. Strzoda, M-C Amann, "VCSEL-based calibration-free carbon monoxide sensor at 2.3 μm with in-line reference cell," Appl. Phys. B **102**, 381 (2011).
23. Z. Qu, R. Ghorbani, D. Valiev, and F. M. Schmidt, "Calibration-free scanned wavelength modulation spectroscopy application to H2O and temperature sensing in flames," Opt. Express **23**, 16492–16499 (2015).

1. Introduction

Tunable diode laser absorption spectroscopy (TDLAS) based gas sensors have transitioned in the past few decades from a laboratory based gas sensor into a practical sensor for field applications, such as combustion monitoring [1–4], flow measurement [5, 6], fuel cell monitoring [7] and environmental monitoring [8–10]. In TDLAS, the emission wavelength of a frequency-agile narrow-linewidth diode laser is current-tuned using a low frequency current waveform across a strong and ideally well-isolated rotational-vibrational absorption line of

a target gas. Accurate recovery of the absorption line shape is performed by detecting the spectral variation of the transmitted light intensity. Important properties of the gas such as concentration, pressure and temperature can then be extracted by fitting a simulated line shape to the experimental line shape. This method known as direct detection is simple to implement and is particularly attractive because faithful recovery of the absolute line shape makes this measurement absolute in nature. Direct detection however has low sensitivity and is therefore not useful in many applications. Wavelength modulation spectroscopy (WMS) is the variant of the TDLAS technique that is most widely used to achieve high sensitivity. In WMS, the diode laser is modulated with a high frequency sinusoid superimposed on a low frequency ramp or a sinusoidal waveform that is used to scan the center wavelength. The interaction of the laser output with the absorption line of the target gas results in the generation of signals at various harmonics of the modulation frequency, f_m. A lock-in amplifier (LIA) is used to filter out the n^{th} harmonic signal and shift it to the baseband, isolating the information bearing signal from noise sources at frequencies outside the LIA filter bandwidth. The experimental signal is fitted with a corresponding simulated signal to obtain the gas parameters. In many field applications, there are significant variations in the measured signals that are not due to variation in gas parameters but due to systematic issues such as vibrations, contamination of the optics and drift in laser characteristics due to temperature variation or aging. These variations result in errors in the measurement of gas parameters unless they are eliminated altogether or accounted for through a calibration step. Periodic re-calibration in industrial systems is not a viable solution because post-installation access is limited in many cases. For such applications two distinct calibration-free techniques are widely used [11–20]. The 1f-normalised 2f technique (2f/1f) [11–13] and its extension to n^{th} harmonic, i.e. $nf/1f$ technique where $n \geq 2$ [14, 15], has been shown to be immune to absorption-independent transmission losses that are outside the pass band of the $1f$ and nf modulation frequencies. Apart from being immune to absorption-independent systematic issues such as light scattering, variable coupling and unintended beam deflection caused by vibrations, it has been shown that this method is also applicable at high pressures when the adjacent absorption lines blend with each other.

However, when non-absorbing regions of the spectrum are available within the spectral tuning range of the laser, an alternate and equally efficient method was recently demonstrated [16]. An added advantage of the new WMS method, proposed in that paper, is its ability to extract all the relevant laser parameters in-situ and in real-time. In this paper we report on a detailed investigation of the overall utility and limitations of this method using three different lasers, namely a 5250 nm continuous wave distributed feedback quantum cascade laser (cw-DFB-QCL) for the measurement of nitric oxide, a 2004 nm vertical cavity surface emitting laser (VCSEL) for the measurement of carbon dioxide (CO_2) and a 1650 nm distributed feedback (DFB) laser for the measurement of methane (CH_4). These results clearly demonstrate that this technique is widely applicable to the three types of lasers that are most commonly used in WMS. Results for the third harmonic along with the second harmonic WMS using these three lasers are also presented in this paper to demonstrate that this technique is not limited to 2f WMS but can readily be extended to higher harmonic WMS measurement.

Traditionally 2f WMS was preferred over 1f WMS because of the low absorption-independent background RAM. Harmonics higher than second harmonic were not preferred because of their lower signal strength. However, for lasers that have large nonlinearity in their intensity versus current characteristics (such as the cw-DFB-QCL laser used in this study) a large absorption-independent background is a part of the 2f signal. This large absorption-independent background leads to early saturation of the detection electronics and limits the accuracy of measurement. For higher harmonics, although the signal strength itself decreases, the ratio of the signal to the absorption-independent background RAM increases. Hence if

the intensity versus current characteristics is significantly nonlinear, harmonics higher than the second harmonic may provide more accurate results, especially for low concentration measurements. The final choice of the harmonic ($2^{nd}, 3^{rd}, 4^{th}$ etc) depends on the extent of nonlinearity in the intensity versus current characteristics curve. For each of the three lasers used in this study, the characteristic curve is well approximated by a cubic polynomial. Fourth and higher order terms were insignificant and have been ignored here. Since for these three lasers, the third harmonic signal has negligible background, therefore results only up to the third harmonic have been presented here. However, it is emphasized that the method described in this paper can readily be extended to higher harmonics should it be necessary to do so.

2. Theoretical discussion of nf WMS

2.1. Fundamentals of WMS

In this section we recapitulate the general mathematical framework that is used to describe the genesis and interaction of signals in WMS. The notation is intentionally chosen to be similar to that commonly used in other papers on WMS. When the input current of an injection current-modulated semiconductor laser is modulated at a frequency $\omega_m = 2\pi f_m$, the intensity of the emitted light, I_{in}, is given by

$$I_{in} = I + \Delta I_1 \cos(\omega_m t) + \Delta I_2 \cos(2\omega_m t + \psi_2 - \psi_1) + \Delta I_3 \cos(3\omega_m t + \psi_3 - \psi_1) + ... \quad (1)$$

and the emission frequency, ν, is given by

$$\nu = \nu_\prime + \Delta\nu \cos(\omega_m t - \psi_1). \quad (2)$$

where I is the DC intensity, ΔI_1, ΔI_2 and ΔI_3 are the 1^{st}, 2^{nd} and 3^{rd} order IM amplitudes respectively (higher order IM amplitudes must be considered if their magnitudes become significant due to the nonlinearity in the intensity versus current characteristics of the laser), ψ_1, ψ_2 and ψ_3 are the phase differences between the frequency modulation (FM) and the 1^{st}, 2^{nd} and 3^{rd} order IM components respectively, and $\Delta\nu$ is the FM amplitude. The terms I, ΔI_1, ΔI_2, ΔI_3, ψ_1, ψ_2, ψ_3 and $\Delta\nu$ in Eq. (1) and Eq. (2) are functions of the DC laser frequency $\nu_\prime$ and may vary significantly over the laser scan range. This is shown later in this paper. Using the Beer-Lambert relation the relative transmission can be expressed as

$$\tau(\nu) = I_{out}(\nu)/I_{in}(\nu) = \exp[-\alpha(\nu)] \quad (3)$$

where $\alpha(\nu)$ is the absorbance and can be expressed in the form of a Fourier cosine series

$$\alpha[\nu_\prime + \Delta\nu \cos\omega t] = \sum_{n=0}^{\infty} H_n(\nu_\prime, \Delta\nu) \cos(n\omega t) \quad (4)$$

where the function $H_n(\nu_\prime, \Delta\nu)$ is the n^{th} Fourier coefficient. The output intensity I_{out} is then the product of the input intensity and the expression for the transfer characteristics i.e. Eq. (1) and Eq. (3). To obtain the two component signals of a LIA locked at the n^{th} harmonic, this product is multiplied by $\cos(n\omega t)$ and $\sin(n\omega t)$ and only the DC terms are retained to simulate the LIAs low pass filtering action. Considering only the first, second and third harmonic signals, the final components are given by Eq. (5) to Eq. (10). A phasor representation of these components for a typical DFB laser is shown in Fig. 1. The relative magnitudes of the phasors depend on the intensity versus current characteristics of the laser, while the values of ψ_1, ψ_2 and ψ_3 depend on the laser and also on the modulation frequency, modulation amplitude and the DC bias current.

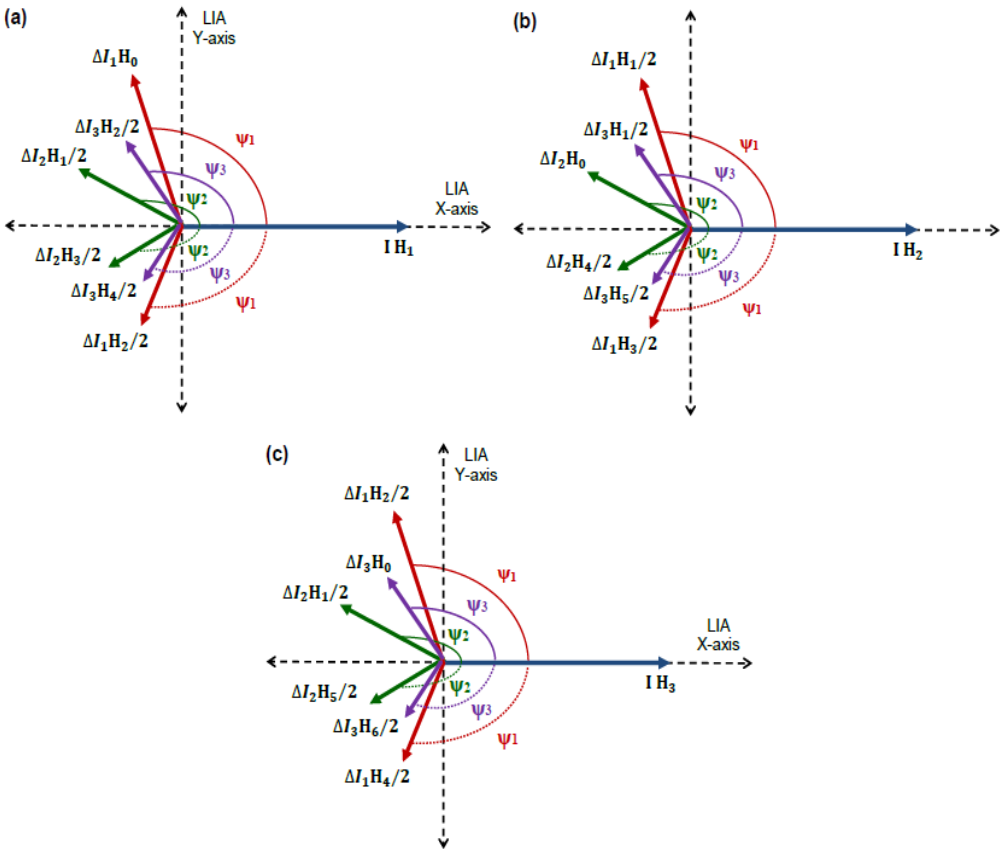

Fig. 1. Phasor representation of (a) first harmonic signal components (b) second harmonic signal components (c) third harmonic signal components.

$$X_{1f} = IH_1 + \Delta I_1 \left(H_0 + \frac{H_2}{2}\right)\cos\psi_1 + \frac{\Delta I_2}{2}(H_1 + H_3)\cos\psi_2 + \frac{\Delta I_3}{2}(H_2 + H_4)\cos\psi_3 \quad (5)$$

$$Y_{1f} = \Delta I_1 (\left(H_0 - \frac{H_2}{2}\right)\sin\psi_1 + \frac{\Delta I_2}{2}(H_1 - H_3)\sin\psi_2 + \frac{\Delta I_3}{2}(H_2 - H_4)\sin\psi_3 \quad (6)$$

$$X_{2f} = IH_2 + \frac{\Delta I_1}{2}(H_1 + H_3)\cos\psi_1 + \Delta I_2 \left(H_0 + \frac{H_4}{2}\right)\cos\psi_2 + \frac{\Delta I_3}{2}(H_1 + H_5)\cos\psi_3 \quad (7)$$

$$Y_{2f} = \frac{\Delta I_1}{2}(H_1 - H_3)\sin\psi_1 + \Delta I_2 \left(H_0 - \frac{H_4}{2}\right)\sin\psi_2 + \frac{\Delta I_3}{2}(H_1 - H_5)\sin\psi_3 \quad (8)$$

$$X_{3f} = IH_3 + \frac{\Delta I_1}{2}(H_2 + H_4)\cos\psi_1 + \frac{\Delta I_2}{2}(H_5 + H_1)\cos\psi_2 + \Delta I_3 \left(H_0 + \frac{H_6}{2}\right)\cos\psi_3 \quad (9)$$

$$Y_{3f} = \frac{\Delta I_1}{2}(H_2 - H_4)\sin\psi_1 + \Delta I_2\,(H_1 - H_5)\sin\psi_2 + \Delta I_3\left(H_0 - \frac{H_6}{2}\right)\sin\psi_3 \tag{10}$$

The magnitude of the n^{th} harmonic can be obtained by

$$R_{nf} = \sqrt{X_{nf}^2 + Y_{nf}^2} \tag{11}$$

In the $nf/1f$ method the ratio of the magnitudes of the nf and the $1f$ signal (R_{nf}/R_{1f}) is obtained experimentally and compared with its simulated value to extract the gas concentration and pressure. From Eq. (5) to Eq. (10), the laser parameters I, ΔI_1, ΔI_2, ΔI_3, ψ_1, ψ_2, ψ_3 and $\Delta\nu$ must be accurately characterized to simulate the $nf/1f$ signal. Although laser characterization in itself is not difficult, variations in these parameters due to calibration drift, temperature variations and aging introduce errors in the measurement. Recently Qu et al. [23], proposed a method that does not require pre-characterization of $I(\nu_t)$, $\Delta I_1(\nu_t)$ and $\psi_1(\nu_t)$. However, other parameters still need to be pre-characterized.

2.2. Methodology for nf WMS measurement using the new method

This section presents a brief description of the methodology for the in-situ real-time measurement of laser parameters. A more elaborate experimental and theoretical description of the measurement of each of these parameters is presented later in section 4. The transmitted laser intensity, I, in the absence of the gas, is obtained by digitally filtering out the high frequency components from the signal received at the photodetector and then interpolating from the non-absorbing wings. A part of the laser output is passed through a fiber interferometer or a solid etalon to carry out wavelength referencing and to obtain the value of $\Delta\nu$. The values of ΔI_1, ΔI_2, ΔI_3, ψ_1, ψ_2 and ψ_3 are obtained by interpolating between the non-absorbing wings of the X and Y components of the demodulated 1f, 2f and 3f signals. Using this method, values of all these laser parameters are obtained at each point along the scan. Hence measurements made using this method are not affected by the variation of these parameters over the wavelength scan range because they are accounted for in the simulations. The in-situ and real-time measurement of all relevant laser parameters also ensures that the measurements are not affected by rapid non-absorbing variations such as those due to light scattering, beam steering, vibrations and window fouling, or by slow variations such as those due to temperature variations, calibration drift and aging of the devices.

2.3. Measurement at the phase quadrature modulation frequency

When the laser is operated at its phase quadrature modulation frequency (f_q), the phase, ψ_1, between the 1^{st} order IM and the FM is 90^o. At f_q the two 1^{st} order IM-dependent distorting signal components, $\Delta I_1 H_1/2$ and $\Delta I_1 H_3/2$, for the second harmonic detection are orthogonal to the main detection axis signal, IH_2, and therefore do not affect the measurement [16]. Similarly, for the third harmonic detection the two 1^{st} order IM dependent distorting signal components, $\Delta I_1 H_2/2$ and $\Delta I_1 H_4/2$, are orthogonal to the main detection axis signal, IH_3, and therefore do not affect the measurement. The values of f_q are generally found to be on the order of 1 MHz [17]. Operation at such high frequencies requires wide bandwidth laser drivers and lock-in detection electronics. However, for the 1650 nm DFB laser used in this study, a significantly lower f_q of 125.5 kHz was obtained [18]. The absorption-independent background RAM, which heavily distorts the recovered 2f WMS signal for low concentrations, can also be removed by 2f RAM nulling [16, 20].

3. Experimental Setup

Figure 2 shows the generic experimental set-up used in this work. The three lasers were driven with different electronic equipment, the signals were detected with different photodetectors, the gas cells were different and the data acquisition (DAQ) systems comprising the LIA and the digitizer were also different. The specific details of the equipment for experiments with each of the three lasers are given in the following sub-sections. The only difference between these experimental setups and a typical WMS setup is that the transmitted signal detected by the photodetector is also recorded in addition to the nf signals that are subsequently extracted by the LIA.

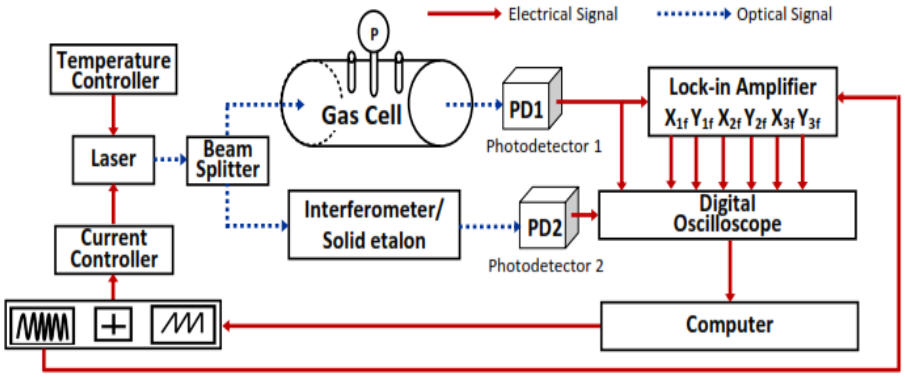

Fig. 2. Schematic of the generic experimental setup used for the implementation of 2f or 3f WMS using this method. Components such as signal generator, laser diode controller, detector, etalon and gas cell are different for each of the three set-up described in this paper.

3.1. Experimental setup for 5250 nm cw-DFB-QCL laser

For the detection of nitric oxide, a free-space coupled cw-DFB-QCL from Alpes Lasers (HHL-286) is driven by a laser diode current and temperature controller (Thorlabs ITC4005). The output of the QCL passes through a 50-50 beam splitter and the transmitted beam enters a 10 cm long stainless steel gas cell with calcium fluoride windows and a digital pressure gauge. The reflected beam passes through a Germanium etalon that has a free spectral range (FSR) of 0.57843 GHz. The light transmitted through the gas cell is detected with a DC-coupled mercury cadmium tellurium (HgCdTe) detector from Infrared Systems Development Corporation (MCT-5-TE3-2.0) that is coupled to a pre-amplifier (MCT1000) of the same make. The signal transmitted through the etalon is detected with a DC-coupled HgCdTe detector from Vigo (PVMI-4TE-8). This signal is used to wavelength reference the time-indexed gas absorption signals and also to obtain the variation of FM amplitude along the wavelength scan. Both the detector outputs are connected to a 2.5 GHz digital storage oscilloscope (DSO) (Agilent Infiniium 54853A). The DSO is connected to a computer through a GPIB interface. In all three cases, a custom LabVIEW programme is used to automate the entire operation of controlling the laser driver electronics, acquiring data from the DSO and the LIA, measurement of laser characteristics, and finally curve fitting to extract the gas parameters.

3.2. Experimental setup for 2004 nm VCSEL laser

For these experiments, a 2004 nm free-space coupled VCSEL from VERTILAS GmbH (VL-2004-1-SQ-A5) is driven by a VCSEL laser diode current and temperature controller (Thorlabs

VITC002). The output from the laser is passed through a collimator (Holmarc HO-CS25-0.8) and then through a 50-50 beam splitter (Newport Corporation CAFBS11) that splits the incoming light into two parts. One part of the incident light passes through a 28 cm long free-space gas cell. The temperature and pressure of the cell are monitored using a PT-100 thermocouple and a digital pressure gauge. The light transmitted through the gas cell is detected by a thermoelectrically-cooled photodetector (Thorlabs PDA10DT-EC) that has a spectral range of 1.2-2.6 μm. The photodetector output is connected through a T connector to a 50 MHz digital LIA (Zurich Instruments HF2LI) and a 500 MHz DSO (Tektronix TDS3054C). This allows both the harmonic signals demodulated by the LIA and the signal detected by the photodetector directly (prior to demodulation) to be viewed on the DSO and recorded to a computer over a GPIB interface. The second part of the light incident on the beam splitter is passed through a solid etalon (Light Machinery OP-2638-16622) that has an FSR of 2.5 GHz and is detected with an InGaAs photodetector (Thorlabs PDA10D-EC).

3.3. Experimental setup for 1650 nm DFB laser

The technique described in this paper was first demonstrated by using a 10 mW distributed feedback (DFB) laser (Toptica Photonics LD-1665-0010-DFB-1) with a nominal emission wavelength of 1650 nm to interrogate the R4 absorption line of CH_4 at 1650.96 nm [16]. The laser is driven by a current controller (Thorlabs LDC 220C) and a temperature controller (Thorlabs TED 200C). The fiber-coupled laser output is split into two parts with a 3 dB coupler (Thorlabs 10202A-50-APC). The output from one arm of the 3 dB coupler passes through the same 28 cm long gas cell mentioned in section 3.2. The second arm of the 3dB coupler is connected to a fiber interferometer that has an FSR of 0.2091 GHz. The rest of the setup is identical to that described in section 3.2.

4. In situ measurement of relevant laser parameters

This section provides a detailed description of the methodology for in-situ real-time extraction of laser parameters. In order to show the extraction of I, ΔI_1, ΔI_2, ΔI_3, ψ_1, ψ_2 and ψ_3 from the transmitted signal received at the photodetector, the set-up described in section 3.3 was used with the gas cell filled with 1% CH_4 sample at 1 bar pressure. The set-up described in section 3.1 was used to show a comparison of ψ_1 obtained using the traditional method and that obtained using this method, with the gas cell filled with 680 ppm nitric oxide at 500 mbar pressure. Measurement of the FM amplitude along the ramp and a comparison of its maximum deviation from the line center value is also shown in section 4.3, for each of the three lasers at the optimum modulation index value of $m = 2.2$.

4.1. Measurement of laser intensity across the wavelength scan

Figure 3(a) shows the transmitted signal detected directly by the photodetector when the 1650 nm DFB laser was modulated at 20 kHz with a modulation amplitude of 10 mA p-p. This signal was low-pass filtered with an FIR digital filter to remove the high-frequency sinusoidal component. The non-absorbing wings of the digitally filtered signal, shown by the blue circular markers in Fig. 3(b), were interpolated to obtain the laser intensity I across the wavelength scan. It should be noted that it does not matter if the use of a high-order filter to retrieve the non-absorbing wings leads to distortion of the absorbing regions of the transmitted signal. This is so because the intensity versus time characteristics or intensity versus current characteristics for most semiconductor lasers does not show significant nonlinearity of order higher than the 2^{nd} or 3^{rd} order. Hence although the absorbing regions of the transmitted signal may get distorted by the filtering action the non-absorbing wings would not be significantly affected.

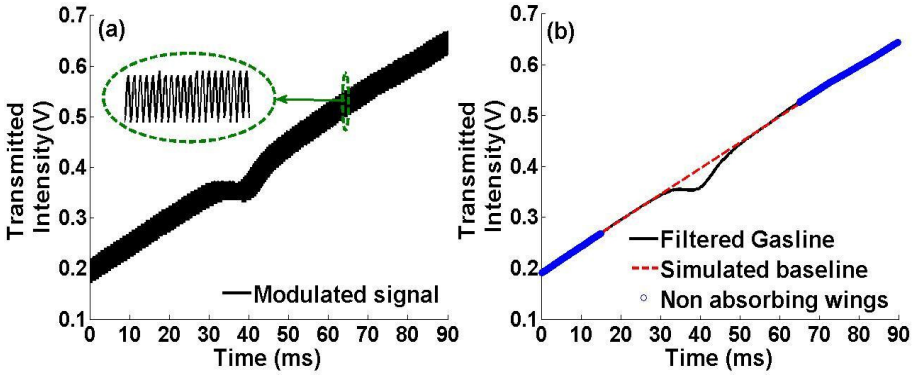

Fig. 3. (a) Modulated output received at the photodetector when the 1650 nm DFB laser was modulated at 20 kHz 10 mA p-p sinusoid superimposed on a 10 Hz 60 mA p-p ramp. (b) Intensity obtained by fitting a baseline to the digitally filtered modulated output signal.

4.2. *Measurement of n^{th} order IM amplitude and its phase differences with respect to the FM component*

When no gas absorption is present, the n^{th} harmonic signal components and its magnitude are given by

$$X_{nf}(no\ gas) = \Delta I_n \cos(\psi_n) \tag{12}$$

$$Y_{nf}(no\ gas) = \Delta I_n \sin(\psi_n) \tag{13}$$

$$R_{nf}(no\ gas) = \Delta I_n \tag{14}$$

These equations are rigorously valid for any wavelength where the gas does not have appreciable absorption. The regions of negligible absorption are highlighted in Fig. 4. The non-absorbing regions of the magnitude of 1f, 2f and 3f signals are shown by the blue circular markers in parts (c), (f) and (i) respectively. Interpolating from these non-absorbing regions 1^{st} order, 2^{nd} order and 3^{rd} order IM amplitudes, i.e. ΔI_1, ΔI_2 and ΔI_3 respectively, were obtained at each point of the scan.

The procedure to determine the phase between n^{th} order IM and FM, ψ_n, at each point of the scan range is described here. The X-axis of the LIA locked at the n^{th} harmonic, is aligned along the IH_n component as shown by the phasor diagram in Fig. 1(a), (b) and (c) and experimentally in Fig. 4(a),(d) and (g) . In the absence of absorption, the signals along the X and Y component of the LIA are given by Eq. (12) and Eq. (13), respectively. The values of $X_{nf}(no\ gas)$ and and $Y_{nf}(no\ gas)$ can be obtained in the presence of the absorbing gas by interpolating from these non-absorbing spectral wings, shown by the blue circular markers in the Fig. 4(a),(b),(d),(e), (g) and (h). The phase ψ_n between the n^{th} order IM and the FM can be obtained by taking the inverse tangent of the ratio of these two signals.

$$\frac{Y_{nf}(no\ gas)}{X_{nf}(no\ gas)} = \frac{\Delta I_n \sin(\psi_n)}{\Delta I_n \cos(\psi_n)} = tan\ (\psi_n) \tag{15}$$

For instance, to obtain the phase between the 2^{nd} order IM and FM, the X component of the signal demodulated at the second harmonic is aligned along the IH_2. Then ψ_2 is obtained by interpolating from the non-absorbing regions of the X and the Y component of the 2f signal and taking their ratio. However, this method of measurement of ψ_n is valid only if the phase of the FM does not vary along the scan range. This method is very simple and computationally

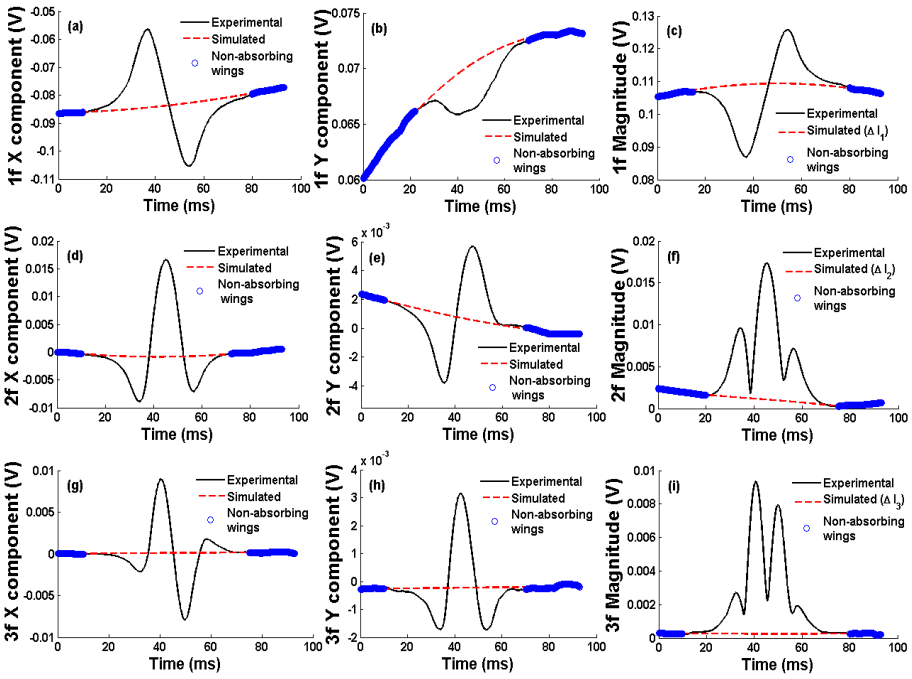

Fig. 4. The 1650 nm DFB laser was modulated at m = 2.2 and the transmitted light through a 1% CH_4 sample at 1 bar pressure was demodulated by a LIA to obtain (a) 1f X-component along IH_1 (b) 1f Y-component orthogonal to IH_1 (c) Magnitude of 1f Signal (d) 2f X-component along IH_2 (e) 2f Y-component orthogonal to IH_2 (f) Magnitude of 2f Signal (g) 3f X-component along IH_3 (h) 3f Y-component orthogonal to IH_3 (i) Magnitude of 3f Signal .

very efficient. However, for some lasers the phase of the FM may vary along the scan range. For such lasers ψ_n must be measured by obtaining the modulated output and the fibre-ring resonator output, simultaneously. The difference between the consecutive peaks of the resonator output is obtained and the maxima and the minima of the difference are used to obtain the inflection points of the FM output. These inflection points are shown by the black star markers in Fig. 5 (b). The magnitude of the frequency difference between any two consecutive peaks of the resonator is equal to the FSR of the resonator. In between the inflection points the frequency value would alternately be monotonically increasing and monotonically decreasing. Hence by using the resonator peaks, the FSR value, and the inflection points, the frequency values at each point where the resonator peak occurs are obtained. The FM output is obtained at each point of the scan range by fitting a sinusoid to these frequency values, as shown in Fig. 5 (c). The FM output is then passed through a software LIA locked at f_m to obtain the phase of the FM output. The modulated output is also passed through a software LIA locked at the n^{th} harmonic of f_m to obtain the phase of the n^{th} harmonic component of the modulated output. The difference between the phase of the n^{th} harmonic component of the modulated output and the FM output provides the value of ψ_n in the non-absorbing regions. Phase values at each point of the scan range are obtained by interpolating from the phase values in the non-absorbing regions.

However, this method of determining the phase requires a low-FSR etalon and a high sampling rate DAQ system and it will also increase the computation complexity. Due to the unavailability of the high sampling rate DAQ, this method could not be tested for the lasers used

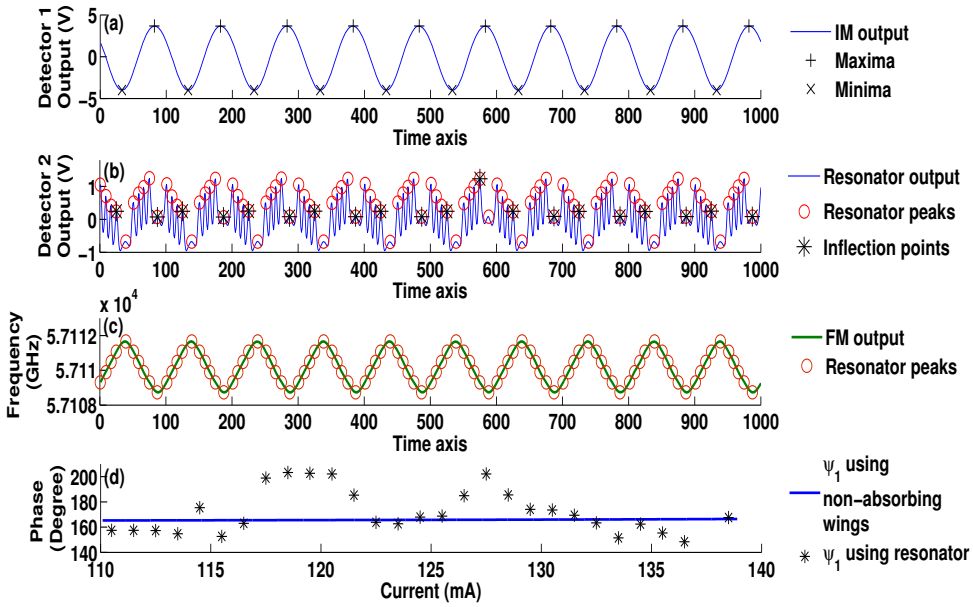

Fig. 5. Using the 5250 nm cw-DFB-QCL modulated at 10 kHz with a 10 mA p-p sinusoidal waveform (a) Intensity modulation output at fixed DC bias (b) Resonator output at fixed DC bias (c) Frequency modulation output at fixed DC bias (d) Comparison of ψ_1 obtained using the resonator output with that obtained using the non-absorbing wings, across the scan range.

in this study. However, in order to compare the two methods, ψ_1 was measured by measuring the modulated output and the fibre-ring resonator output, simultaneously, at fixed DC bias current values (ramp was turned off) of the laser, using the set-up described in section 3 but with the gas cell removed. The DC bias current of the laser was then varied in small increments along the scan range of the laser and ψ_1 was obtained at each of these DC values. It was observed that ψ_1 obtained using the two methods, for the three lasers used in this study, were in agreement with each other. Figure 5 shows a comparison of the two methods using a cw-DFB-QCL that was modulated at 10 kHz with 10 mA p-p sinusoidal waveform. The difference between the inflection points (maxima and minima) of the IM output and that of the FM output, as shown in Fig. 5 (a) and (b), is used to obtain the phase between the 1^{st} order IM output and the FM output. The DC bias of the laser is then varied in 1 mA increments to obtain ψ_1 from 110 mA to 140 mA. Figure 5 (d) shows a comparison of phase between the 1^{st} order IM and FM obtained using the two methods. The accuracy of the traditional method depends strongly on the FSR of the etalon. If there are n number of peaks between two consecutive infection points of the IM then maximum error in measurement of the phase would be $\pm(180/n)^o$. Figure 5 shows that this error is about $\pm\ 22^o$ for the set-up described in this section. This error could be minimized by using an etalon of lower FSR. However, an etalon of lower FSR can be significantly costlier specially in mid-IR region. Another way to reduce this error is by interpolating the phase value for each point of the x-axis. It is observed that obtaining ψ_n using the non-absorbing wings of the nf signal components is a much simpler technique to implement. Its accuracy would only depend on the accuracy of the interpolation of the non-absorbing wings. The accuracy would be higher for larger non-absorbing regions.

4.3. Measuring the FM amplitude along the ramp

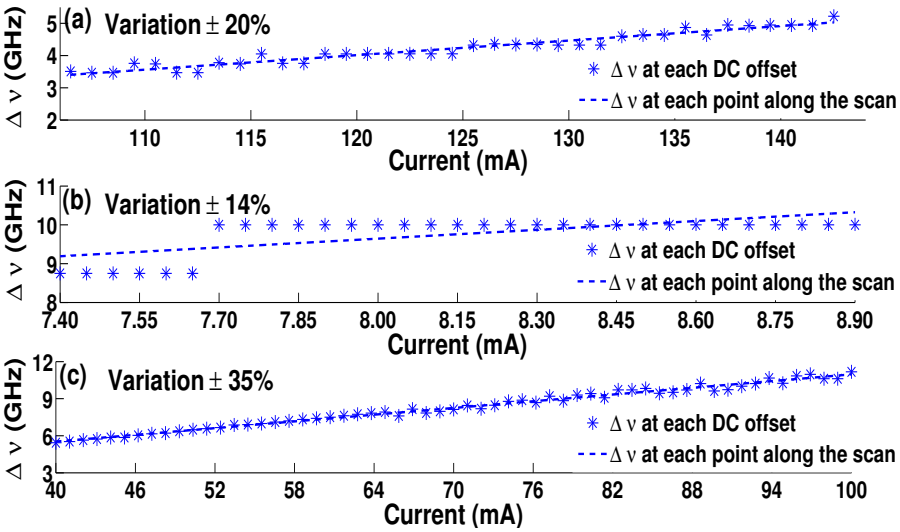

Fig. 6. Variation of FM amplitude along the ramp for (a) 5250 nm cw-DFB QCL (± 20%) (b) 2004 nm VCSEL (± 14%) (c) 1650 nm DFB laser(± 35%).

As discussed in section 4.2, if the FSR of the resonator is small enough and the sampling rate of the DAQ system is large enough then the FM output (Fig. 5 (c)) can be obtained from the resonator output. The FM output obtained is passed through a LIA, locked at f_m, to obtain the magnitude of the 1^{st} order FM output at each point along the current scan range. If there is significant nonlinearity in the frequency versus current characteristics of the laser, the LIA can be locked to the higher harmonics to retrieve the amplitudes of the higher order FM output. However, due to the unavailability of the high sampling rate DAQ system, the DC bias of each of the three lasers was varied in small increments along their respective current scan ranges and the 1^{st} order FM output was obtained at each of these DC values. Figure 6 (a) show that $\Delta\nu$ varies by $\pm$ 20% from the value at the line center for the 5250 nm cw-DFB-QCL when operated at $f_m = 8\ kHz$ with a line center m-value of 2.2 at 0.387 bar pressure. Figure 6 (b) show that $\Delta\nu$ varies by $\pm$ 14%, from the value at the line center for the 2004 nm VCSEL when operated at $f_m = 10\ kHz$ with a line center m-value of 2.2 at 1 bar pressure. Figure. 6 (c) shows that $\Delta\nu$ varies by $\pm$ 35% from the value at the line center for the 1650 nm DFB laser when operated at $f_m = 20\ kHz$ with a line center m-value of 2.2 at 1 bar pressure. The current scan ranges shown in Fig. 6 (a), (b) and (c) correspond to the wavelength scan ranges over which the three lasers used in this study have been scanned as shown in the results presented later (Fig. 8, Fig. 10 and Fig. 12, respectively). It is evident that depending upon the nonlinearity of the current-frequency relationship of the laser there may be significant variations in the FM amplitude across the frequency scan range. The simulation of the 2f signal must therefore account for this variation. Reports [22] have also shown that $\Delta\nu$ of semiconductor lasers varies with temperature and aging. The methodology presented here provides real-time measurement and therefore also takes into account such long-term drift of the FM amplitude. The maximum systematic error in the measured value of $\Delta\nu$ depends on the FSR of the interferometer or the etalon (error $\leq \pm\ FSR/2$). The larger the FSR, the greater is the error in the measurement of $\Delta\nu$. Figure 6 (b) shows that instead of a gradual change in the $\Delta\nu$ value there is a step change at around 7.65 mA DC current value. This is because the overall change in the FM amplitude

for the given ramp current is comparable to the FSR (= 2.5 GHz) of the etalon used.

5. Experimental Results

5.1. Calibration-free 2f and 3f WMS measurement of nitric oxide using 5250 nm cw-DFB-QCL

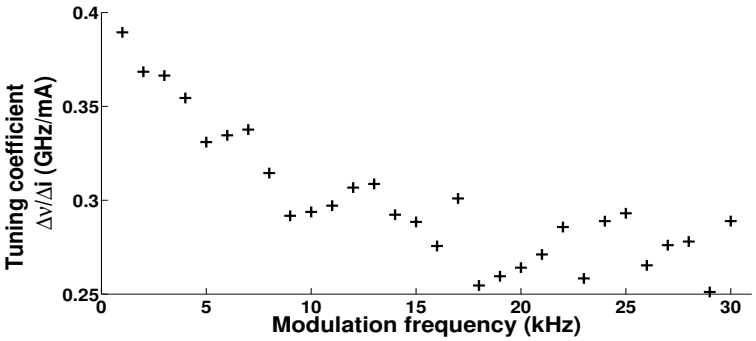

Fig. 7. Variation of tuning coefficient of the 5250 nm cw-DFB-QCL with modulation frequency

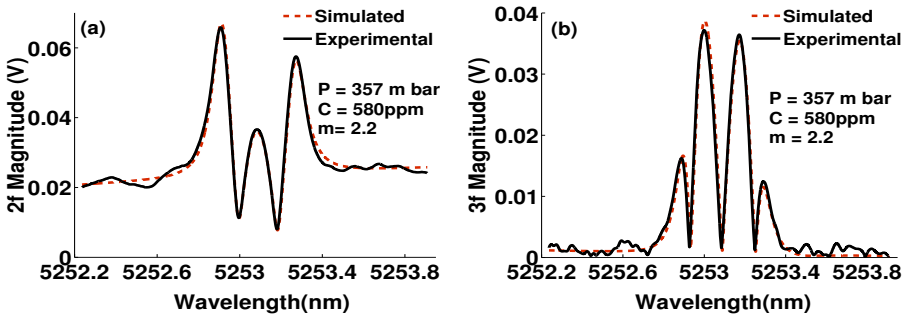

Fig. 8. Experimental and simulated signals at m = 2.2, $f_m = 8\ kHz$ for 580 ppm nitric oxide at 0.357 bar pressure for (a) second harmonic (b) third harmonic.

The 5250 nm cw-DFB-QCL was temperature-tuned (1.53^{o}C) to target the R7 transition of nitric oxide. The laser was modulated with a 8 kHz, 13.5 mA p-p sinusoid (m = 2.2 at 0.387 bar pressure) that was superimposed on a 40 mA p-p ramp (DC bias 122.5 mA). The magnitude of the experimental and the simulated 2f and 3f signals for a 580 ppm nitric oxide sample at 0.357 bar pressure are shown in Fig. 8 (a) and (b) respectively. The excellent agreement between the simulation and the experimental data is evident. As shown in Fig. 8, it can be observed that although the 2f signal is stronger than the 3f signal, it is accompanied by a large absorption independent background RAM which varies across the scan range. This is due to the nonlinearity of the cw-DFB-QCL laser used in this study. Hence the peak height of the 2f WMS signal cannot be considered proportional to the concentration of the gas. This would add to the complexity of measurement and may also lead to errors in measurement especially for low concentrations. However, the 3f WMS signal has an almost negligible absorption-independent

background RAM and therefore the peak of the magnitude of the 3f WMS signal or the peak-to-peak of the X-component of the 3f WMS signal is directly proportional to the concentration of the gas. Figure 7 shows that the tuning coefficient of the cw-DFB-QCL used in this study decreases rapidly with increasing f_m. This implies that the amplitude of the modulating current must be increased to attain the same m-value at higher f_m. The current modulation amplitude could be increased only up to the point where instantaneous current input to the laser does not exceed the maximum current limit of the laser. The laser was therefore modulated at a relatively low modulation frequency of 8 kHz in order to attain the optimum m-value of 2.2. This method cannot be used for measurement of nitric oxide at higher pressures with the current set-up because of the limited tunable range (0.5 nm) and low value of tuning coefficient (0.3145 GHz/mA at 8 kHz) of the laser. In this case it is not the density of the spectrum but the limited tunable range of the laser that restricts this method from being applied at higher pressure. A laser with a wider tunable range would allow this method to be used up to much higher pressure values.

5.2. Calibration-free 2f and 3f WMS measurement of carbon dioxide using 2004 nm VCSEL

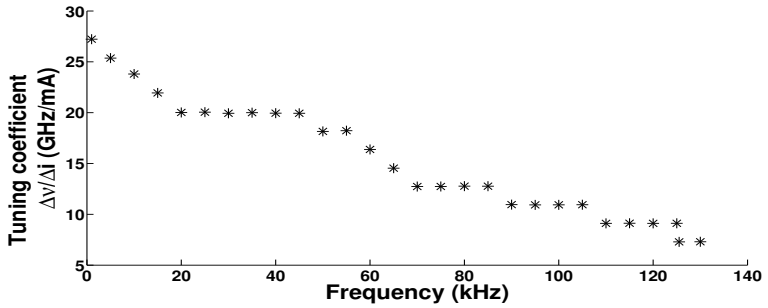

Fig. 9. Variation of tuning coefficient of the 2004 nm VCSEL with modulation frequency.

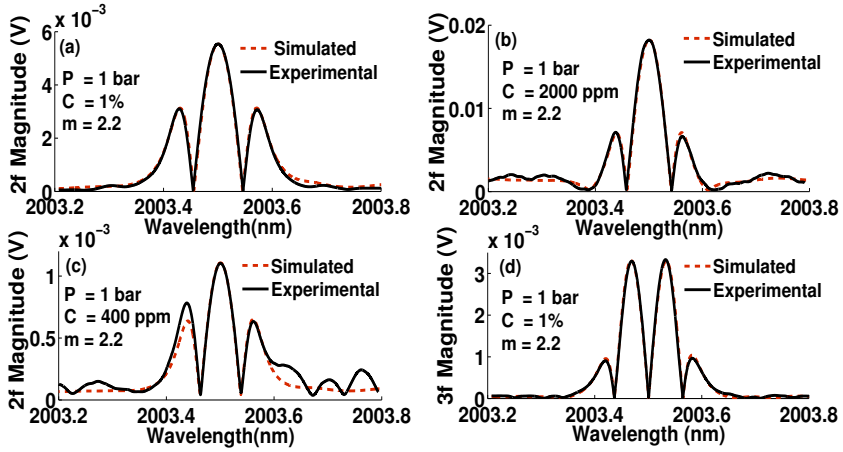

Fig. 10. Experimental and simulated signals at m = 2.2, $f_m = 10kHz$ and 1 bar pressure for (a) 1% CO_2 sample using 2f WMS (b) 2000 ppm CO_2 sample using 2f WMS (c) 400 ppm CO_2 sample using 2f WMS and (d) 1% CO_2 sample using 3f WMS.

The VCSEL was temperature tuned to 2003.5 nm to target the R16 transition of CO_2. The laser was operated at the optimum $m = 2.2$ point by modulating at $f_m = 10$ kHz with a 0.29 mA p-p sinusoid superimposed on a 1.50 mA p-p ramp. Magnitudes of the 2f WMS signals for 1%, 2000 ppm and 400 ppm CO_2 sample at 1 bar pressure are shown in Fig. 10 (a), (b) and (c), respectively. Figure 10 (d) shows the magnitude of the 3f WMS signal for 1% CO_2 sample at 1 bar pressure. It can be observed that the fitting between the simulated and the experimental signals is good. However, for low concentration the etalon noise becomes prominent as shown in Fig. 10 (c). As shown in Fig. 9 the tuning coefficient of the VCSEL used in this study is much higher than that for the cw-DFB-QCL (shown in Fig. 7). The VCSEL's tunable range of about 5 nm is also much higher than the 0.5 nm range of the QCL. However, despite these advantages this method cannot be used for the measurement of CO_2 at pressure values higher than the atmospheric pressure. This is so because blending of the adjacent absorption lines at higher pressures makes it impossible to obtain the non-absorbing wings. Hence for such cases it is the congested nature of the spectrum rather than the lasers tunable range or the tuning coefficient which limits the maximum operating pressure.

5.3. Calibration-free 2f and 3f WMS measurement of methane using 1650 nm DFB laser

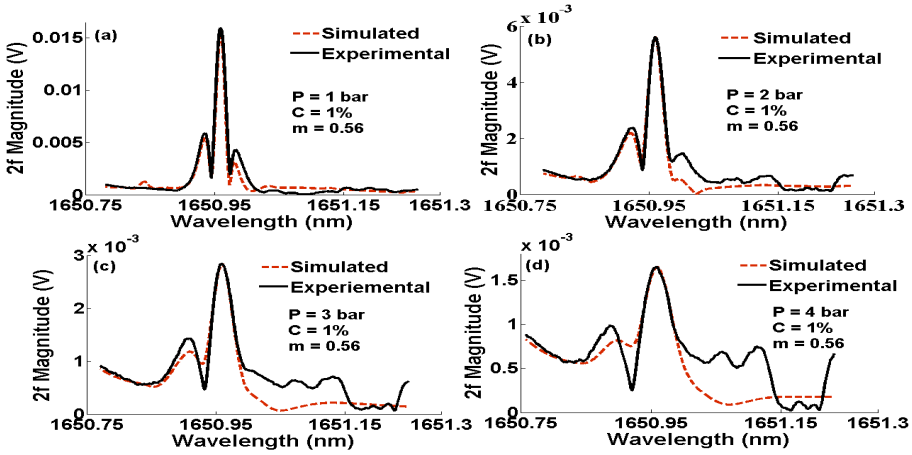

Fig. 11. Experimental and simulated 2f WMS signals at m = 0.56, $f_m = 20kHz$ for 1% CH_4 at pressure values of (a) 1 bar (b) 2 bar (c) 3 bar (d) 4 bar

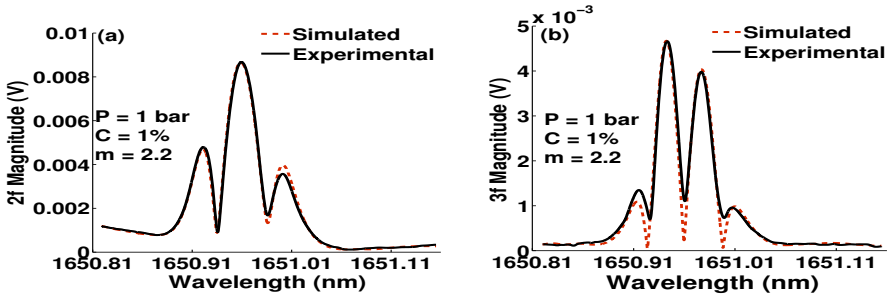

Fig. 12. Experimental and simulated WMS signals at m = 2.2, $f_m = 20kHz$ for 1% CH_4 sample at 1 bar pressure using (a) 2f WMS and (b) 3f WMS.

The 1650 nm DFB laser was operated at a m-value of 0.56 and a modulation frequency of 20 kHz to measure a 1% CH_4 sample at 1-4 bar at 1 bar increments, as shown in Fig. 11 (a), (b), (c) and (d), respectively. It is observed that with the increase in pressure the fit between the simulated and the experimental signals deteriorates. This is mainly because for a given modulation index the 2f signal broadens with the increase in pressure. This leads to a reduction of the available non-absorbing wings which in turn leads to an error in the measurement of laser characteristics that are required for the simulation of 2f or 3f-WMS signal. This problem can be overcome if a more widely tunable laser is used. For instance a typical 1650 nm VCSEL has a tuning range of about 5 nm as compared to 0.5 nm of the DFB laser used in this study and hence can be used to measure CH_4 up to much higher pressure values. Hence for cases such as these where the availability of the non-absorbing wings is not precluded by the spectral interference, the wavelength tuning range of the laser limits the maximum pressure up to which this method can be used for a given m-value. Figure 12(a) and (b) shows the experimental and simulated WMS signals when this method was implemented at the optimum modulation index, $m = 2.2$ at $f_m = 20$ kHz to measure a 1% CH_4 sample at 1 bar pressure, using 2f and 3f WMS respectively.

6. Discussion

In order to simulate the nf WMS signal accurately various laser parameters (I, ΔI_1, ΔI_2, ΔI_3, ψ_1, ψ_2, ψ_3 and $\Delta\nu$) must be either pre-characterized or measured in-situ. Higher order IM terms and their respective phase shifts with respect to the FM also have to be considered if the intensity versus current characteristics of the laser is highly nonlinear. These laser parameters may have a weak or a strong dependence on the instantaneous frequency, ν_i. It is therefore important to measure these parameters at each point of the scan range. The method described in this paper not only measures these laser parameters at each point along the scan range, it continuously monitors these laser parameters. Any change in the output signal due to the rapidly varying non-absorbing losses is accounted for in the simulated signal as well. Also these laser parameters may drift with time due to aging or with temperature variation. In-situ real-time measurement of these parameters ensures that there is no error in the measurement due to such variations. Quantum cascade lasers (QCLs) are very widely used for high-sensitivity, multi-component WMS measurements. QCLs, such as the external cavity quantum cascade laser (ECQCL) used by Chao et al [13] and the cw-DFB-QCL laser used in this study, are known to have much higher nonlinearity in their intensity versus current characteristics as compared to DFB lasers. This results in a large absorption-independent 2f background RAM that varies across the scan range. Higher order WMS signals are weaker than the 2f WMS signal but have a higher signal to the absorption independent background RAM ratio. Hence the 3f WMS for the cw-DFB-QCL laser used in this study has an almost negligible absorption-independent background RAM which helps in avoiding early saturation of the detection electronics and also makes the measurement of the gas concentration using 3f WMS signal easier and less prone to error. Therefore it can be advantageous to use 3f WMS and other higher order WMS for some lasers. The demonstration of 3f WMS using the three different types of lasers shows that the method proposed in this paper is not limited to 2f WMS measurements but can also be used for the measurement of gases using 3f WMS or if required for other higher order WMS measurements. However, as any other method that uses the non-absorbing wings of the absorption spectrum, such as the scanned wavelength direct detection method, the residual amplitude modulation (RAM) method, the phasor decomposition (PD) method and the RAM nulling method, the applicability of this method depends on the availability of the non-absorbing wings which in turn depends on the tuning coefficient and the tunable range of the laser, as well as on the congestion of spectral region of operation. The effort in this paper has been to bring out this

limitation clearly and explicitly. For instance, the cw-DFB-QCL laser used in this study has a very low tuning coefficient and narrow tunable range and therefore cannot be used to measure nitric oxide at a pressure higher than 500 mbar. However, cw-DFB-QCLs are relatively new and more and more advanced QCLs with wider tunable range and higher tuning coefficient are coming up. VCSELs on the other hand have a much wider tunable range as well as a much higher tuning coefficient, and are better suited for measurement of gases that have spectrally isolated absorption lines. A good example of such an isolated line is the CH_4 absorption line at 1650.8 nm. This method could be used up to much higher pressure values if this line is chosen. However, this method will not work at high operating pressures if the spectrum is too congested, even if the tuning coefficient is large and the tunable range of the laser is wide. For instance, the measurement of CO_2 at 2004 nm using a VCSEL will be limited to about 1 bar because of the spectral congestion in that region due to several CO2 and ammonia lines. For a given application, one would need to assess the extent of this problem by simulating the absorption spectrum at the expected operation pressure to check if non-absorbing wings are available. If only concentration measurements are required (such as in breath analysis), the sample gas could be brought down to a lower pressure at which the non-absorbing wings are available and then this method can be applied. However, if the application requires an in-situ real-time high pressure measurement of a gas and if the non-absorbing wings are not available at those pressures, the traditional $nf/1f$ method would be a more suitable option.

7. Conclusion

This paper presents a detailed explanation of an alternate calibration-free WMS method with in-situ real-time characterization of laser parameters at each point along the scan range. The technique is shown to be applicable to three different types of lasers viz. cw-DFB-QCL, VCSEL and DFB lasers. Results for 2f and 3f WMS are presented here for each of these three lasers. If the spectral region around the selected absorption line is congested, this technique would work only up to a certain pressure value that would depend on the level of congestion. There are many applications however, where only a few gases are known to be present and these gases may have well separated lines. In such cases where the availability of non-absorbing spectral wings may not be a problem, it is the tunable range of the laser that would place an upper limit on the pressure values up to which the technique could be used. Widely tunable semiconductor lasers are readily available nowadays and isolated spectral lines are available in various parts of the spectrum as well. This should therefore not be a major limitation although more investigations are required on this aspect. A particular merit of this technique is that it can be incorporated into existing WMS systems without any disruption or major modifications because the experimental set-up is essentially identical to most WMS set-ups.

All data supporting this research are openly available from `http://dx.doi.org/10.15129/82e23d9e-4502-4018-900c-a73d497f8a0c`

Acknowledgement

This work was supported in part by the Department of Science and Technology, Government of India under the grant SR/S3/EECE/0112/2010. A part of this work was also supported by the Fiber Laser Imaging of gas Turbine Exhaust Species (FLITES) project and an EPSRC grant EP/J002178/1. We are also thankful to Ms. Zarin A. S. from IIT Gandhinagar for verifying some of the results presented in this paper.